Scattering From Isotropic Connected Wire Medium Metamaterials: Three-, Two-, and One-Dimensional Cases

Ebrahim Forati, *Student Member, IEEE*, and George W. Hanson, *Fellow, IEEE*

***Abstract*—Scattering problems involving wire media are computationally intensive due to the spatially dispersive nature of homogenized wire media. In this work, an integro-differential equation based on a transport formulation is proposed instead of the convolution-form integral equation that directly arises from spatial dispersion. The integro-differential equation is much faster to solve than the convolution equation form, and its effectiveness is confirmed by solving several examples in one-, two-, and three-dimensions. As experimental confirmation of both the integro-differential equation formulation and the homogenized wire medium parameters, several isotropic connected wire medium spheres have been fabricated on a rapid-prototyping machine, and their measured extinction cross sections compared with simulation results. Wire parameters (period and diameter) are varied to the point where homogenization theory breaks down, which is reflected in the measurements.**

***Index Terms*—Artificial plasma, integral equations, metamaterial, scattering, wire medium.**

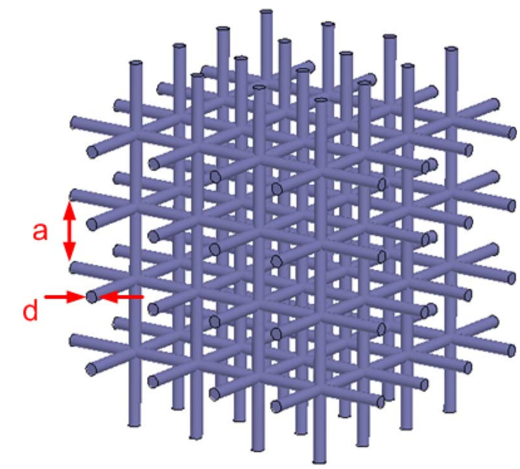

Fig. 1. Depiction of an isotropic connected wire medium having period a and wire diameter d.

I. Introduction

An isotropic connected wire medium (ICWM) is a square lattice of connected wires, as depicted in Fig. 1. ICWMs can act as an artificial plasma with negative permittivity and a relatively low (e.g., GHz) plasma frequency [1]. The basic concept of a wire medium as an artificial plasma has been known since the 1960s [2], [3]. However, recent studies have demonstrated interesting applications which were unknown before, as well as considerable complications arising from their spatially-dispersive nature [4], [5]. Some recent applications have included super lensing and subwavelength imaging [6]–[10], cloaking [11], shielding [12], and antenna applications [13], [14].

Maxwell's equations, along with constitutive (material related) parameters, continuity equations, and appropriate boundary conditions, fully describe electromagnetic interactions between a source and a medium. However, defining appropriate material parameters is often difficult, especially for metamaterials and particularly for spatially-dispersive materials. It is common to model materials which, upon homogenization, are nonlocal, in terms of a momentum-space wavevector-dependent conductivity and/or permittivity. This leads to convolution-type integral equations (IEs) in the space domain, and in three-dimensions the solution of these equations necessitates solving six-fold integrals (three over the convolution variables and three over the space variables), or even nine-fold integrals if the space-domain material parameters cannot be obtained in analytical form. The difficulty of doing this is likely the reason that the problem of scattering from three-dimensional wire medium objects such as spheres has not been presented.

In this work, building on [15] and [16], we show that for an ICWM the problem can be formulated as a three-fold integro-differential equation, which is much faster to solve, and we provide for the first time results for scattering from a three-dimensional wire medium object, an ICWM sphere. We confirm the presented theory experimentally by measurements of the extinction cross section of several ICWM spheres, fabricated on a rapid-prototyping machine. We show that their measured extinction cross sections compare well with simulation results assuming a nonlocal homogenized material response (recast as a drift-diffusion equation involving "local" material parameters; a different "local" model that nevertheless encompasses spatial dispersion is given in [17]). We examine experimentally the point at which the homogenization theory breaks down as wire period is increased. The integro-differential equation method is also applied to one- and two-dimensional scattering problems,

Manuscript received December 05, 2012; revised February 13, 2013; accepted March 09, 2013. Date of publication March 22, 2013; date of current version July 01, 2013.

The authors are with the Department of Electrical Engineering, University of Wisconsin-Milwaukee, Milwaukee, WI 53211 USA (e-mail: george@uwm.edu).

Color versions of one or more of the figures in this paper are available online at http://ieeexplore.ieee.org.

Digital Object Identifier 10.1109/TAP.2013.2254455

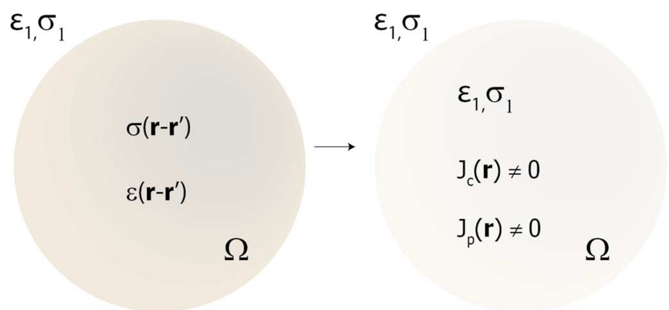

Fig. 2. Volume equivalence principle for nonlocal materials. Left side: the original problem of a nonlocal medium having volume Ω immersed in a local background medium. Right: the equivalent problem of a homogeneous local medium having, within the volume Ω, nonzero polarization and conduction currents.

and the results are verified by comparison with previous results. In the following we are considering nonmagnetic isotropic wire media, and the time convention (suppressed) is $e^{j\omega t}$.

II. Conventional/Direct Approach for Nonlocal Scattering Problems

Before describing the transport-based integro-differential equation, in this a section we describe what might be called the direct integral equation method for nonlocal materials, where we use the term direct since it results from the basic definition of nonlocal response. We use the volume equivalence principle to replace a nonlocal medium (characterized by $\sigma(\mathbf{r}-\mathbf{r}')$ and/or relative permittivity $\epsilon(\mathbf{r}-\mathbf{r}')$ and having domain Ω) embedded in an infinite local medium characterized by ϵ_1, σ_1 with a homogeneous space characterized by ϵ_1, σ_1 but having equivalent volume conduction ($\mathbf{J}_{\rm c}$) and polarization ($\mathbf{J}_{\rm p}$) currents in the domain Ω, as shown in Fig. 2. Note that although the volume equivalence principle is usually applied to local and linear materials, it is easy to show that it applies to very general nonlocal and even nonlinear materials [18]. Although we use the material parameters for a translationally invariant medium, the additional boundary condition described below rigorously accounts for the material boundary [19].

For example, assume the case of a material having a nonlocal conduction and polarization response, $\mathbf{J}_{\rm c}(\mathbf{q}) = (\sigma(\mathbf{q}) - \sigma_1)\mathbf{E}(\mathbf{q})$ and $\mathbf{J}_{\rm p}(\mathbf{q}) = j\omega\epsilon_0(\epsilon(\mathbf{q}) - \epsilon_1)\mathbf{E}(\mathbf{q})$, where we assume the spatial transform pair $\mathbf{r} \leftrightarrow \mathbf{q}$. The corresponding space-domain relations are

$$\mathbf{J}_{\rm c}(\mathbf{r}) = \int (\sigma(\mathbf{r}-\mathbf{r}') - \sigma_1\delta(\mathbf{r}-\mathbf{r}'))\mathbf{E}(\mathbf{r}')\, d\Omega', \qquad (1)$$

$$\mathbf{J}_{\rm p}(\mathbf{r}) = j\omega\epsilon_0 \int (\varepsilon(\mathbf{r}-\mathbf{r}') - \varepsilon_1\delta(\mathbf{r}-\mathbf{r}'))\mathbf{E}(\mathbf{r}')\, d\Omega' \qquad (2)$$

where (1) is a generalized ohm's law for the effective conduction response and (2) gives a similar relationship for the effective polarization response. Given that the relationship between current and field is given in terms of a three-fold integral

$$\mathbf{E}(\mathbf{r}) = -j\omega\mu \int \underline{\mathbf{G}}_{\rm ee}(\mathbf{r},\mathbf{r}') \cdot \mathbf{J}(\mathbf{r}')\, d\Omega' \qquad (3)$$

where $\underline{\mathbf{G}}_{\rm ee}$ is the dyadic Green's function defined as (63) in Appendix D, then the convolution-type integral equations to be solved are

$$\begin{aligned}\mathbf{J}_{\rm c}(\mathbf{r}) = &\int (\sigma(\mathbf{r}-\mathbf{r}') - \sigma_1\delta(\mathbf{r}-\mathbf{r}')) \\ &\times \left[\left(-j\omega\mu \int \underline{\mathbf{G}}_{\rm ee}(\mathbf{r}',\mathbf{r}'') \cdot \mathbf{J}_{\rm eq}(\mathbf{r}'')\, d\Omega''\right)\right. \\ &\left. + \mathbf{E}^i(\mathbf{r}')\right] d\Omega' \end{aligned} \qquad (4)$$

and

$$\begin{aligned}\mathbf{J}_{\rm p}(\mathbf{r}) = j\omega\epsilon_0 &\int (\varepsilon(\mathbf{r}-\mathbf{r}') - \varepsilon_1\delta(\mathbf{r}-\mathbf{r}')) \\ &\times \left[\left(-j\omega\mu \int \underline{\mathbf{G}}_{\rm ee}(\mathbf{r}',\mathbf{r}'') \cdot \mathbf{J}_{\rm eq}(\mathbf{r}'')\, d\Omega''\right)\right. \\ &\left. + \mathbf{E}^i(\mathbf{r}')\right] d\Omega' \end{aligned} \qquad (5)$$

for all $\mathbf{r} \in \Omega$, where $\mathbf{J}_{\rm eq} = \mathbf{J}_{\rm c} + \mathbf{J}_{\rm p}$.

Equations (4) and (5) are what we term the direct convolution form integral equations, since they arise directly from the convolution forms (1)–(2). These involve computationally intensive six fold integrals. Furthermore, determining the space-domain material parameters $\sigma(\mathbf{r})$ and $\epsilon(\mathbf{r})$ from the momentum representations $\sigma(\mathbf{q})$ and $\epsilon(\mathbf{q})$ represents another three-fold integration unless the inversion to the space domain can be performed analytically. In the absence of that ability, the IEs involve nine-fold integrals, which may be impossible to compute from a practical standpoint.

It is worth noting that in the much simpler local isotropic case we have $\mathbf{J}_{\rm c}(\mathbf{r}) = (\sigma - \sigma_1)\mathbf{E}(\mathbf{r})$ and $\mathbf{J}_{\rm p}(\mathbf{r}) = j\omega\epsilon_0(\epsilon - \epsilon_1)\mathbf{E}(\mathbf{r})$, such that

$$\begin{aligned}&\frac{\mathbf{J}_{\rm c}(\mathbf{r})}{\sigma - \sigma_1} \\ &\quad = -j\omega\mu \int \underline{\mathbf{G}}_{\rm ee}(\mathbf{r},\mathbf{r}') \cdot \mathbf{J}_{\rm eq}(\mathbf{r}')\, d\Omega' + \mathbf{E}^i(\mathbf{r})\end{aligned} \qquad (6)$$

and

$$\begin{aligned}&\frac{\mathbf{J}_{\rm p}(\mathbf{r})}{j\omega\epsilon_0(\epsilon - \epsilon_1)} \\ &\quad = -j\omega\mu \int \underline{\mathbf{G}}_{\rm ee}(\mathbf{r},\mathbf{r}') \cdot \mathbf{J}_{\rm eq}(\mathbf{r}')\, d\Omega' + \mathbf{E}^i(\mathbf{r})\end{aligned} \qquad (7)$$

for all $\mathbf{r} \in \Omega$. These can simply be added together to form a single, three-fold IE

$$\frac{\mathbf{J}_{\rm eq}(\mathbf{r})}{\sigma_{\rm c}} = -j\omega\mu \int \underline{\mathbf{G}}_{\rm ee}(\mathbf{r},\mathbf{r}') \cdot \mathbf{J}_{\rm eq}(\mathbf{r}')\, d\Omega' + \mathbf{E}^i(\mathbf{r}) \qquad (8)$$

where $\sigma_{\rm c} = (\sigma - \sigma_1) + j\omega\epsilon_0(\epsilon - \epsilon_1)$ is the combined composite complex conductivity that describes all conduction and polarization effects. Perhaps more often, (8) is expressed in terms of a combined effective relative permittivity $\epsilon_{\rm c} = \epsilon - \epsilon_1 + (\sigma - \sigma_1)/j\omega\epsilon_0$ as

$$\mathbf{E}(\mathbf{r}) = \left(\omega^2\mu\epsilon_0\varepsilon_{\rm c} \int \underline{\mathbf{G}}_{\rm ee}(\mathbf{r},\mathbf{r}') \cdot \mathbf{E}(\mathbf{r}')\, d\Omega' + \mathbf{E}^i(\mathbf{r})\right) \qquad (9)$$

for all $\mathbf{r} \in \Omega$, which is the usual volume integral equation for local penetrable scatterers [20].

Returning to the nonlocal case, we consider an ICWM constructed from imperfectly-conducting wires characterized by $\varepsilon_m = 1 - \omega_m^2/(\omega(\omega - j\Gamma))$, where ω_m and Γ are the plasma frequency and damping frequency of the metal, respectively. When homogenization is appropriate (i.e., when the wire period is much smaller than wavelength [21]), both conduction and polarization effects can be contained in a single nonlocal relative permittivity [1]

$$\underline{\epsilon}(\mathbf{q}, \omega) = \mathbf{1}\varepsilon_h - \kappa \left(\mathbf{1} - \frac{1}{q^2 + l_0 \left(\frac{\varepsilon_h k_p^2}{\varepsilon_m - \varepsilon_h} \frac{1}{f_v} - k_h^2 \right)} \mathbf{qq} \right) \quad (10)$$

where

$$\kappa = \left(\frac{k_0^2}{k_p^2} - \frac{1}{\varepsilon_m - \varepsilon_h} \frac{1}{f_v} \right)^{-1} \quad (11)$$

$f_v = \pi r^2/a^2$ is the volume fraction of the wires, r is the wire radius, a is the wire period, $k_h = \omega\sqrt{\mu_0 \varepsilon_0 \varepsilon_h} = k_0\sqrt{\varepsilon_h}$ is the wavenumber in the dielectric supporting the wires, $k_p = \omega_p/c$ is the plasma wavenumber given by $(k_p a)^2 \cong 2\pi/\ln((a^2)/(4r(a-r))) \cong 2\pi/(\ln((a)/(2\pi r))+0.5275)$; see ([1], (11)) for the exact expression, and $l_0 = 3/(1 + 2k_p^2/\beta_1^2)$, where

$$\frac{1}{\beta_1^2} = 2\left(\frac{a}{2\pi}\right)^2 \sum_{n=1}^{\infty} \frac{\left[J_0\left(\frac{2\pi r}{a} n\right)\right]^2}{n^2} \quad (12)$$

and where J_0 is the zeroth-order Bessel function. As discussed in [1], this expression is very accurate below the effective plasma frequency, which, for $\varepsilon_h \sim 1$ is

$$\frac{1}{\omega_{p,\text{eff}}^2} = \varepsilon_h \left(\frac{1}{\omega_m^2 f_v} + \frac{1}{k_p^2 c^2} \right). \quad (13)$$

If ε_h differs considerably from unity the effective transverse permittivity is not Drude-like and is given by a quadratic form obtained from setting the transverse permittivity to zero. The isotropic wire medium permittivity (10) reduces to the simpler form [22]

$$\underline{\epsilon}(\mathbf{q}, \omega) = \mathbf{1}\varepsilon_h - \frac{k_p^2}{k_0^2} \left(\mathbf{1} - \frac{1}{q^2 - l_0 k_h^2} \mathbf{qq} \right) \quad (14)$$

when $|\varepsilon_m| \to \infty$, i.e., as the wire conductivity becomes infinite. The direct (conventional) method would consist of determining $\underline{\epsilon}(\mathbf{r})$ and using that in the six-fold IE (5); it appears that scattering from three-dimensional wire media has not been considered, likely because of this complication.

III. Integro-Differential Equation—The Drift-Diffusion Approach

In [15], a transport treatment of a nonlocal wire medium was developed, leading to a drift diffusion equation that relates conduction current, electric field, and charge density as

$$\mathbf{J}_{\mathrm{c}}(\mathbf{r}) = \sigma \mathbf{E}(\mathbf{r}) - D\nabla\rho_{\mathrm{c}}(\mathbf{r}) \quad (15)$$

in which σ is the conductivity and D is the diffusion parameter. Although the material parameters σ and D are wavevector-independent, (15) is a nonlocal expression since the gradient samples the spatial region near the point $\mathbf{r}$ [16]. For the ICWM, the equivalent conductivity and diffusion parameters are [15]

$$\begin{aligned} \sigma &= \sigma^{\text{ICWM}} \\ &= j\omega\varepsilon_0 \left(\frac{1}{(\varepsilon_m - \varepsilon_h) f_V} - \frac{\omega^2}{\beta_p^2 c^2} \right)^{-1} \quad (16) \\ D &= D^{\text{ICWM}} \\ &= j\omega \left[l_0 \left(\frac{\varepsilon_h \beta_p^2}{(\varepsilon_m - \varepsilon_h) f_V} - \frac{\varepsilon_h \omega^2}{c^2} \right) \right]^{-1}. \quad (17) \end{aligned}$$

In this formulation, the response of the wire medium is the conduction response, and if the wires are in the same material as the background environment ($\epsilon_h = \epsilon_1$) there is no polarization response, in which case, using (15), Maxwell's equations, and continuity equation, we obtain

$$\begin{aligned} \mathbf{J}_{\mathrm{c}}(\mathbf{r}, \omega) = \sigma \Bigg[&-j\omega\mu \int \underline{\mathbf{G}}_{\mathrm{ee}}(\mathbf{r}, \mathbf{r}') \cdot \mathbf{J}_{\mathrm{c}}(\mathbf{r}')\, d\Omega' \\ &+ \mathbf{E}^i(\mathbf{r}) \Bigg] + \frac{D}{j\omega} \nabla\nabla \cdot \mathbf{J}_{\mathrm{c}}(\mathbf{r}) \quad (18) \end{aligned}$$

for all $\mathbf{r} \in \Omega$. We refer to this as the drift-diffusion (DD) result. This integro-differential formulation involves only three-fold integrals, and differentiation. For solutions involving the expansion of the conduction current in a set of basis functions, taking the derivative of the basis functions is very easy to implement; obviously, the chosen basis function should be twice-differentiable.

If the wires are supported by a material having permittivity different than the background permittivity, then we need to solve the coupled DD system [15]

$$\mathbf{J}_{\mathrm{c}}(\mathbf{r}) = \sigma[\mathbf{E}^{sca}(\mathbf{r}) + \mathbf{E}^i(\mathbf{r})] + \frac{D}{j\omega} \nabla\nabla \cdot \mathbf{J}_{\mathrm{c}}(\mathbf{r}) \quad (19)$$

$$\mathbf{J}_{\mathrm{p}}(\mathbf{r}) = j\omega\varepsilon_0(\varepsilon(\mathbf{r}) - 1)[\mathbf{E}^{sca}(\mathbf{r}) + \mathbf{E}^i(\mathbf{r})] \quad (20)$$

for all $\mathbf{r} \in \Omega$, where

$$\mathbf{E}^{sca}(\mathbf{r}) = -j\omega\mu \int \underline{\mathbf{G}}_{\mathrm{ee}}(\mathbf{r}, \mathbf{r}') \cdot (\mathbf{J}_{\mathrm{c}}(\mathbf{r}') + \mathbf{J}_{\mathrm{p}}(\mathbf{r}'))\, d\Omega'. \quad (21)$$

In terms of complexity, these are three-fold equations, although they are coupled as also occurs for the local case of both permittivity and permeability contrast [23]. Note that these equations reduce to the usual local integral equations when $D = 0$.

In solving both the convolution-form IEs (4)–(5) and the transport-based DD form (18) or (19)–(20) the additional boundary condition that needs to be enforced is (see, e.g., [24], [1], [15])

$$\mathbf{J}_{\mathrm{c}} \cdot \hat{\mathbf{n}} = 0 \quad (22)$$

where $\hat{\mathbf{n}}$ is the unit vector normal to the surface of the region Ω.

In Sections IV-A and IV-B, we solve one-dimensional and two-dimensional examples involving both polarization and conduction current, and in the three-dimensional sphere examples

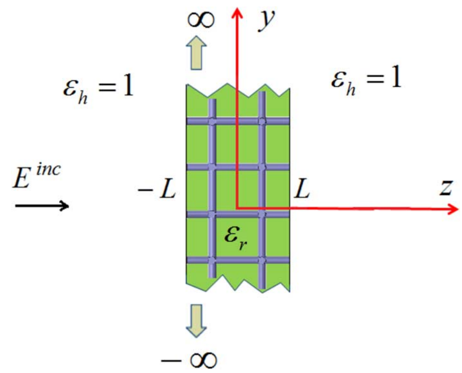

Fig. 3. Wire medium slab with host relative permittivity of ε_r in air.

we assume ($\epsilon_h = \epsilon_1$) and therefore need to consider only conduction current, to avoid unnecessary complications and concentrate on the validation of the method. For the one-dimensional example the new approach leads to a closed form analytical solution even though there are coupled polarization and conduction currents. In Section IV-B, we show that for a two-dimensional wire medium slab the new approach gives the same results as the analytical solution in [1]. In Section IV-C, we apply the formulation to the three-dimensional problem of a sphere of wire medium with different size and wire parameters, and we compare the result with a nonlocal Mie theory and measurement. The strong advantage of this new formulation is that for geometries other than spheres the integro-differential formulation yields a tractable method only involving three-fold integrals (of course, nonlocal Mie theory can only be used to validate the sphere geometry).

IV. Examples

A. One-Dimensional Example

A one-dimensional example based on the new transport formulation was considered in [15], and here we briefly summarize the result, as well as compare with a different method of solution. Consider a slab of ICWM extending to infinity in the x- and y-directions, and extending from $-$L to L in the z direction, as shown in Fig. 3.

We assume a quasi-static incident field $E^{\rm inc}$ which is constant and z-directed; this can be considered to be the field between capacitor plates far-removed from the slab. The wires are immersed in a dielectric host medium having relative permittivity ε_r. For this geometry, solving the DD equations (19)–(21) leads to (23) and (24) for equivalent conduction current and charge density inside the wire medium slab (see Appendix A),

$$J_{\rm c}(z) = \frac{j\omega\sigma\varepsilon_0}{\sigma + j\omega\varepsilon_0\varepsilon_r} \times \left[1 - \frac{\cosh\left(\sqrt{\frac{\sigma + j\omega\varepsilon_0\varepsilon_r}{\varepsilon_0\varepsilon_r D}}z\right)}{\cosh\left(\sqrt{\frac{\sigma + j\omega\varepsilon_0\varepsilon_r}{\varepsilon_0\varepsilon_r D}}L\right)}\right] E^{\rm inc} \tag{23}$$

$$\rho(z) = \frac{\sigma\varepsilon_0}{\sigma + j\omega\varepsilon}\sqrt{\frac{\sigma + j\omega\varepsilon}{D\varepsilon}} \times \frac{\sinh\left(\sqrt{\frac{\sigma + j\omega\varepsilon}{D\varepsilon}}z\right)}{\cosh\left(\frac{\sigma + j\omega\varepsilon}{D\varepsilon}L\right)} E^{\rm inc} \tag{24}$$

in which σ and D are given by (16) and (17), respectively. For perfect electrical conductor (PEC) wires, (23) and (24) simplify to

$$J_{\rm c}(z) = \frac{j\omega\varepsilon_0\beta_p^2}{\beta_p^2 - \varepsilon_r\beta_0^2} \times \left[1 - \frac{\cosh\left(\sqrt{\left(\beta_p^2 - \beta_0^2\varepsilon_r\right) l_0} z\right)}{\cosh\left(\sqrt{\left(\beta_p^2 - \beta_0^2\varepsilon_r\right) l_0} L\right)}\right] E^{\rm inc} \tag{25}$$

$$\rho(z) = \beta_p^2\varepsilon_0\sqrt{\frac{l_0}{\beta_p^2 - \beta_0^2\varepsilon_r}} \times \frac{\sinh\left(\sqrt{\left(\beta_p^2 - \beta_0^2\varepsilon_r\right) l_0} z\right)}{\cosh\left(\sqrt{\left(\beta_p^2 - \beta_0^2\varepsilon_r\right) l_0} L\right)} E^{\rm inc}. \tag{26}$$

There does not seem to be a previous one-dimensional wire medium case with which to compare this solution. However, to demonstrate the applicability of this method we can consider a different diffusive (i.e., spatially-dispersive) material, an n-type semiconductor. This has been considered in [25] under the same excitation as in Fig. 3. There, the solution was obtained by numerically solving coupled transport-Poisson (TP) equations. Here we consider the same material except using the proposed drift-diffusion model. For a semiconducting slab, (23) and (24) are valid using [16]

$$D = \frac{k_B T}{m_e(j\omega + \gamma)} \left[\frac{\mathrm{Am}^2}{C}\right] \tag{27}$$

$$\sigma = \frac{Ne^2}{m_e(j\omega + \gamma)} \left[\frac{\mathrm{S}}{m}\right] \tag{28}$$

where m_e is the effective electron mass, N is the donor doping density, T is temperature in Kelvin, k_B is Boltzmann's constant, and γ is the damping frequency. We consider a slab having thickness $L = 100$ nm and $f = 1$ THz, with $\varepsilon_r = 11.9$, $\gamma = 4.6$ THz, $m_e = 0.26\, m_{e0}$ (m_{e0} is the free-space electron mass), $T = 300$ K, and $E^{\rm inc} = 100$ V/m, which corresponds to the example in [25].

Fig. 4 shows the real part of the charge distribution for three different dopant concentrations using (24) and its comparison with the results reported in [25] using a numerical solution of the coupled transport-Poisson equations. It is evident that the two methods are in complete agreement.

B. 2-D Example

As a two dimensional example, consider the geometry depicted in Fig. 5, where a TM-polarized wave is obliquely incident with angle of θ_i on a slab of wire medium with equivalent parameters D and σ.

After reducing (18) to two dimensions and using the collocation method we can find the induced current inside the slab and thus the scattered (reflected and transmitted) field. The reduced 2-D equations are

$$\sigma E_y^i(z) = \left\{1 + \frac{Dk_y^2}{j\omega}\right\} J_y(z) - \frac{\sigma k_y}{\omega\varepsilon_0}\frac{\partial}{\partial z}\int_0^L g(z,z')J_z(z')\,dz' + \frac{j\sigma k_z^2}{\omega\varepsilon_0}\int_0^L g(z,z')J_y(z')\,dz' - \frac{Dk_y}{\omega}\frac{\partial}{\partial z}J_z(z) \tag{29}$$

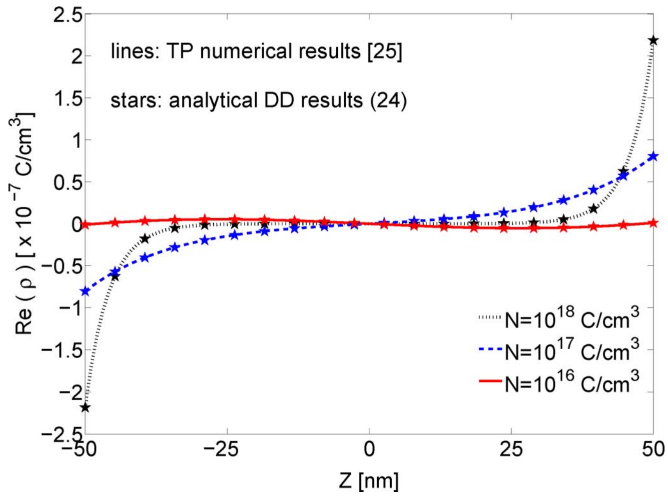

Fig. 4. Real part of the charge distribution inside a nonlocal semiconductor slab for three different dopant densities using the drift diffusion formulation and the coupled transport-Poisson formulation [25].

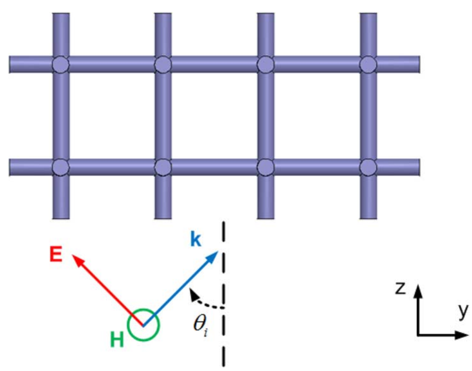

Fig. 5. Wire medium slab infinite in the x- and y-directions.

$$\begin{aligned}\sigma E_z^i(z) &= -\frac{Dk_y}{\omega}\frac{\partial}{\partial z}J_y(z) - \frac{\sigma k_y}{\omega\varepsilon_0}\frac{\partial}{\partial z}\int_0^L g(z,z')J_y(z')\,dz' \\ &+ \frac{j\sigma}{\omega\varepsilon_0}\left(k^2+\frac{\partial^2}{\partial z^2}\right)\int_0^L g(z,z')J_z(z')\,dz' \\ &+ \left\{1-\frac{D}{j\omega}\frac{\partial^2}{\partial z^2}\right\}J_z(z) \end{aligned} \quad (30)$$

where

$$g(z,z') = g(z-z') = \frac{e^{-jk_z|z-z'|}}{2jk_z} \quad (31)$$

$$k_y = k_0\sin(\theta_i), \quad k_z = k_0\cos(\theta_i) = \sqrt{k_1^2-k_y^2}. \quad (32)$$

These were solved using the basis functions

$$J_y(z) = \sum_{n=1}^{N} a_n \sin\left(n\frac{\pi}{L}z\right) + \sum_{n=0}^{N} b_n \cos\left(n\frac{\pi}{L}z\right) \quad (33)$$

$$J_z(z) = \sum_{n=1}^{N} c_n \sin\left(n\frac{\pi}{L}z\right). \quad (34)$$

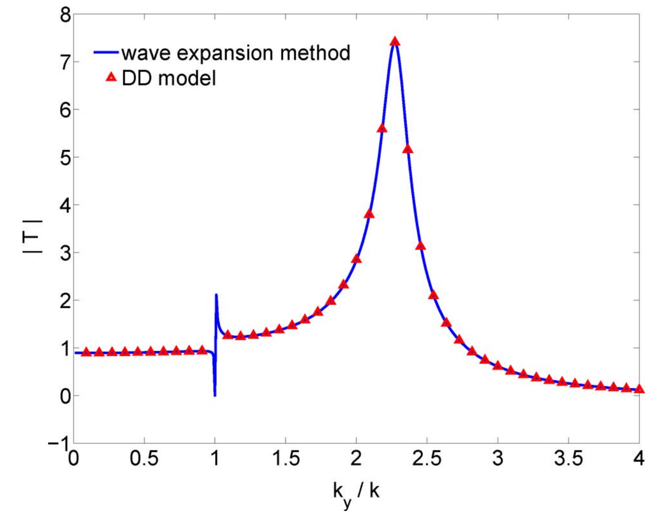

Fig. 6. Comparison of the transmission coefficient of a wire medium slab using the integro-differential drift diffusion method and the wave expansion method of [1].

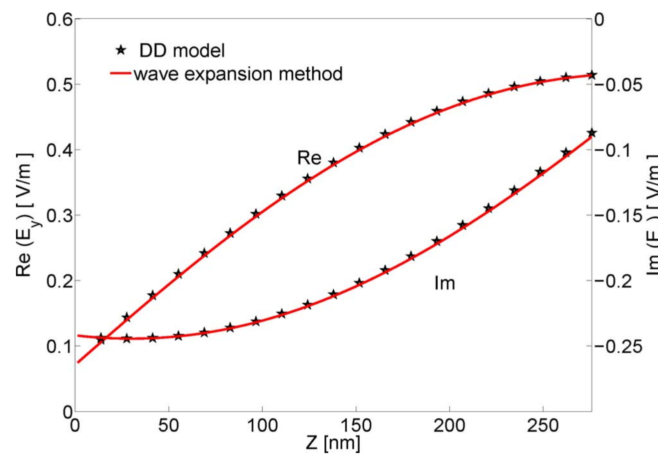

Fig. 7. Internal field E_y of a wire medium slab using the integro-differential drift diffusion method and the wave expansion method of [1].

Fig. 6 shows the transmission coefficient as a function of k_y/k_0 for a slab thickness of 276 nm, $f = 76.1$ THz, $\varepsilon_h = 1$, wire period $a = 276$ nm, $r = 8.25$ nm, and wire permittivity $\varepsilon_m = -810 - j50$ using the drift diffusion formulation and the wave expansion method detailed in [1]; that approach [1] was to use (10) for permittivity and to define induced and scattered fields inside and outside of the slab with unknown coefficients, and match the boundary conditions.

As a more general example, let us assume that the host dielectric of the wire medium has permittivity $\varepsilon_r = 11.9$. In this case we need to solve the coupled system of equations (19)–(21). The resulting two-dimensional formulation and basis function expansions are given in Appendix B. The internal electric fields of this slab are shown in Figs. 7 and 8, which demonstrate that the presented method is in complete agreement with the method of [1].

C. 3-D Example (Spherical Objects)

The two-dimensional example has been solved in the past using other methods. The most significant aspect of the presented formulation is the ability to solve three-dimensional wire-medium problems, which have not been previously

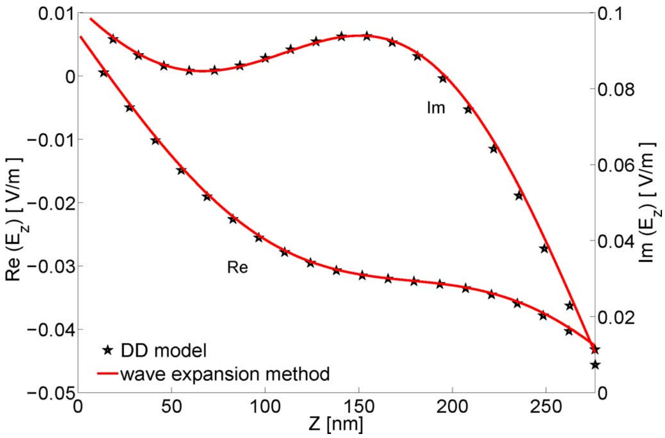

Fig. 8. Internal field E_z of a wire medium slab using the integro-differential drift diffusion method and the wave expansion method of [1].

Fig. 9. Wire medium spheres fabricated using a rapid prototyping machine. All spheres have 50-mm diameter except the far-right sphere, which has diameter 25 mm.

treated. Towards this end, we consider spherical geometries since they are perhaps the simplest three-dimensional case, and they also admit a nonlocal Mie solution [26] which can be used for comparison. Of course, the presented integro-differential formulation is applicably to three-dimensional objects having arbitrary geometries, whereas the nonlocal Mie solution we use for comparison is only applicable to spheres.

1) Formulation: We consider an isotropic wire medium with an air host, and solve (18). In Appendix C, it is shown that any realizable electromagnetic vector quantity inside a nonlocal material can be expanded in terms of

$$\mathbf{M}(\mathbf{r},m,n) = \nabla \times \hat{\mathbf{r}}\psi_{\mathrm{H}}(\mathbf{r},m,n) \tag{35}$$

$$\mathbf{N}(\mathbf{r},m,n) = \frac{1}{k_{\mathrm{tr}}}\nabla \times \nabla \times \hat{\mathbf{r}}\psi_{\mathrm{E}}(\mathbf{r},m,n) \tag{36}$$

$$\mathbf{L}(\mathbf{r},m,n) = \nabla\psi_{\rho}(\mathbf{r},m,n) \tag{37}$$

in which

$$\psi_{\mathrm{H,E}}(\mathbf{r},m,n) = j_n(k_{\mathrm{tr}}r)\begin{Bmatrix}\cos(m\varphi)\\ \sin(m\varphi)\end{Bmatrix} P_n^m(\cos(\theta)) \tag{38}$$

$$\psi_{\rho}(\mathbf{r},m,n) = j_n(\alpha r)\begin{Bmatrix}\cos(m\varphi)\\ \sin(m\varphi)\end{Bmatrix} P_n^m(\cos(\theta)) \tag{39}$$

$$k_{\mathrm{tr}} = \omega\sqrt{\mu\epsilon_0\left(\varepsilon - j\frac{\sigma}{\omega\epsilon_0}\right)} \tag{40}$$

$$\alpha = j\sqrt{\frac{\sigma + j\omega\epsilon_0\varepsilon}{\epsilon_0\varepsilon D}} \tag{41}$$

where $P_n^m(x)$ is the associated Legendre polynomial and $\mathbf{r}$ is the radial vector in spherical coordinates; $r = |\mathbf{r}|$.

These set of functions form a complete set in $L^2(\Omega)$ space where $\Omega = [0,L]^3 \subset \mathbb{R}^3$. The $\mathbf{L}$ functions can be set to zero for expansions of magnetic fields, but are necessary for electric fields and conduction current expansions for $\mathbf{r} \in \Omega$.

Assuming that the incident field is y-directed and is propagating in the z-direction, we may simplify (38) and (39) as [27]

$$\psi_{\mathrm{H,E}}(\mathbf{r},n) = j_n(k_{\mathrm{tr}}r)\sin(\varphi)P_n^1(\cos(\theta)) \tag{42}$$

$$\psi_{\rho}(\mathbf{r},n) = j_n(\alpha r)\cos(\varphi)P_n^1(\cos(\theta)). \tag{43}$$

Therefore, a complete expansion for the conduction current is

$$\mathbf{J}_{\mathrm{c}}(\mathbf{r}) = \sum_n (c_{1n}\mathbf{M}(\mathbf{r},n) + c_{2n}\mathbf{N}(\mathbf{r},n) + c_{3n}\mathbf{L}(\mathbf{r},n)). \tag{44}$$

After inserting (44) into (18) and using the point matching technique, the unknown expansion coefficients c_{in}, $i = 1,2,3$, can be found (more details are provided in Appendix D).

The obtained current is then used to calculate the scattered field using (21). The extinction cross section σ^{ext} of the object can be found using the optical theorem [28], which expresses the extinction cross section of an arbitrarily shaped object in terms of the forward scattered electric field:

$$\sigma^{\mathrm{ext}} = \frac{4\pi}{k^2}\mathrm{Im}\left(\frac{kr}{E_0 e^{jkr}}\mathbf{E}_s^{\parallel}\right) \tag{45}$$

where $\mathbf{E}_s^{\parallel}$ is the far scattered field in the forward direction co-polarized with the incident field, and k is the wavenumber in the host medium external to the scatterer. The optical theorem is usually proved for objects consisting of local materials, but it is simple to repeat the same derivation for nonlocal materials.

2) Simulation and Measurement Results: For comparison with the presented theory, wire medium spheres were fabricated using a rapid prototyping machine (dimension Elite 3-D Printer). The resulting "wires" are P430 ABSplus, which is a plastic material with $\varepsilon_r = 2.53$ (measured in our lab at 2.7 GHz using a split post dielectric resonator (SPDR) [29]). The resulting wire mesh is self-supporting, and is coated with silver paint [30] to form conducting wires. This process results in a several micron thick conductive layer on the insulating "wire" support, so we can consider the resulting wires as PEC at microwave frequencies.

Six different wire medium spheres are examined in this section, as shown in Figs. 9–11. For convenience, we designate each sphere with a three part label $D(\#1)a(\#2)d(\#3)$ in which #1 is the sphere diameter, #2 is the wire period, and #3 is the wire diameter, all in millimeters. For example, D50a4d1 indicates a sphere with diameter 50 mm, wire period 4 mm, and wire diameter 1 mm.

Note for purposes to be discussed later we fabricated two different D50a12d2 spheres as shown in Fig. 11. To distinguish between these we labeled one of them with an extra "C" at its end (i.e., D50a12d2C), which indicates that it has wires crossing at the center. Fig. 11 clarifies the difference between D50a12d2 and D50a12d2C.

The experimental configuration is shown in Fig. 12, consisting primarily of an anechoic box (C), two x-band horns (A), and an E8361A Agilent network analyzer (D). A Styrofoam pedestal (F) is used to support the sphere, and strings (B) are

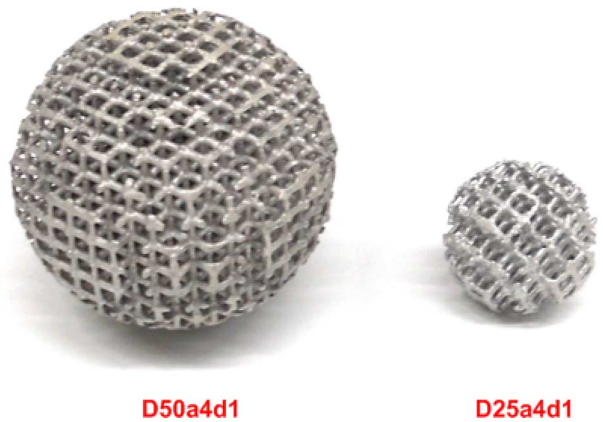

Fig. 10. Close-up of the 50-mm and 25-mm wire medium spheres, both having period 4 mm.

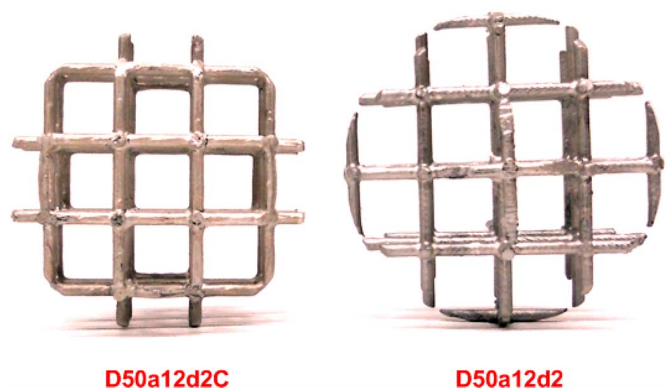

Fig. 11. Close-up of the D40a12d2 and D40a12d2C spheres. Both have the same diameter, period, and wire thickness, but the latter sphere (C) has wires crossing at the center, whereas the other sphere does not.

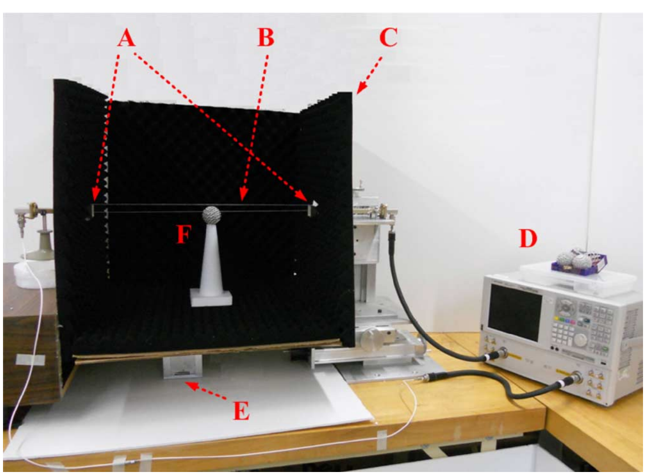

Fig. 12. Measurement setup. A: x-band horn antennas, B: strings for alignment, C: microwave absorbers, D: E8361A Network analyzer, E: height adjustment, F: WM sphere on a Styrofoam pedestal.

used to align the object between the horns. After measuring the forward scattered field using a 25-mm diameter brass sphere for calibration, the optical theorem (45) is used to find the extinction cross section, which is the same as the scattering cross section in our case since the spheres are considered lossless. In order to validate the measurement setup, we considered a variety of metal and plastic spheres of different sizes. In all cases very

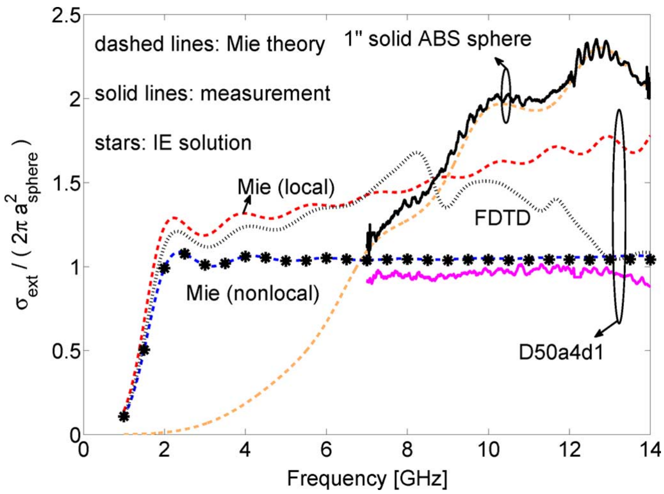

Fig. 13. Normalized measured and theoretical extinction cross sections of the D50a4d1 wire medium sphere and of a plastic sphere.

good agreement with the known extinction cross section was found (one such validation is shown in Fig. 13).

Fig. 13 shows the result of the measurement for the D50a4d1 sphere, and its comparison with the integro-differential DD method (18) using eight expansion terms, a nonlocal Mie theory solution [26] (some simple algebra allows us to express the parameters in [26] in terms of the diffusion constant and conductivity used here. For convenience, the final expressions for the nonlocal Mie coefficients are given in Appendix E), and a finite-difference time domain commercial code (Lumerical, [31]). We also show the result from a local Mie theory (setting $D = 0$), which is not expected to be accurate but which we include just to show the influence of spatial dispersion. In Fig. 13, we also include, as validation of the measurement procedure, a comparison between measurement and Mie theory [27] for an ABSplus solid plastic sphere (which is a local material), also fabricated by the rapid prototyping machine. Measurements are only shown for 7–14 GHz, which is the approximate range of the horn antennas. Results are normalized by twice the geometric cross-sectional area of the spheres (a_{sphere} is the radius of the sphere), which is the high-frequency asymptotic value for PEC spheres [27].

From Fig. 13 it can be seen that the integro-differential DD formulation is in excellent agreement with the nonlocal Mie result (which can be considered to be an exact analytical solution for the homogenized problem), and these are in good agreement with the measurement. The local treatment of the wire medium (e.g., ignoring the wavevector dependence of the permittivity, or, equivalently, setting the diffusion parameter $D = 0$) is seen to be in poor agreement with the nonlocal theory and measurement, highlighting the importance of spatial dispersion for this problem.

The FDTD commercial package was run on a 142 node computer cluster for the actual wire mesh sphere. However, it did not generate very accurate results, although great effort was made to obtain a convergent solution. Extensive numerical tests of spheres at various frequencies and for different wire periods showed that in some cases the FDTD solution more closely resembled the local solution, and in other cases it more closely

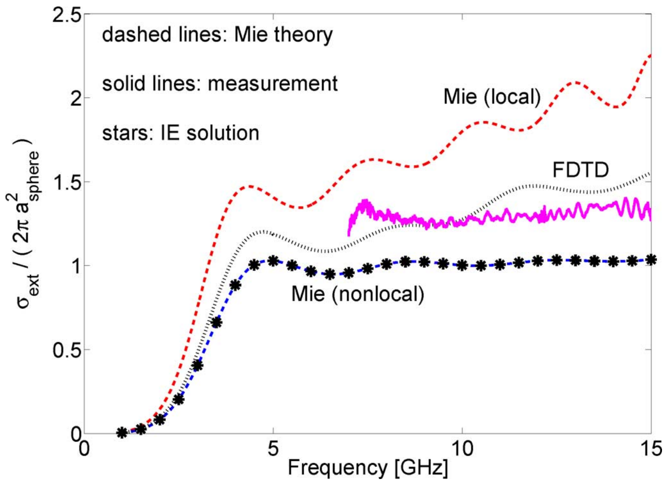

Fig. 14. Normalized measured and theoretical extinction cross sections of the D25a4d1 sphere.

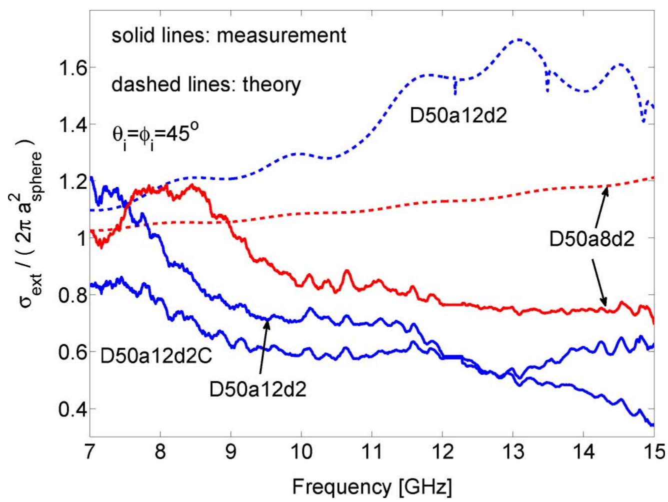

Fig. 15. Normalized measured and theoretical extinction cross sections of the D50a8d2, D50a12d2, and D50a12d2C spheres. Because of the large wire periods, homogenization theory becomes inapplicable in most of the measurement range.

resembled the nonlocal solution—the FDTD solution was often between the local and nonlocal results. We are not sure why the FDTD solution was inaccurate, although it can be noted that the geometry is relatively complex. Lumerical technical support indicated that our FDTD model was correct, and should produce accurate results. Grid spacing was 0.1 mm, which is 0.0046λ at 14 GHz. We attempted to use other commercial codes for comparison as well, but these were not installed on the cluster and we did not have enough memory to run the simulations.

As a rough estimate of computation times, the Mie solution can be considered as essentially instantaneous, the integro-differential equation solution requires a few minutes for calculation, and the FDTD method typically takes 6–8 hours on the 142-node computer cluster.

Fig. 14 shows similar results for the D25a4d1 sphere; note that in this case the normalized cross-section approaches its asymptotic value at approximately 5 GHz, as compared to 2 GHz for the larger sphere. Also, since this sphere is smaller, we only need four terms in (44) to solve the integro-differential DD equation. For this smaller sphere the agreement between nonlocal theory and measurement is still fairly good, but is somewhat poorer than for the larger 50-mm sphere. We attribute this to the fact that the larger sphere forms a relatively smoother spherical surface compared to the 25-mm sphere, in the sense that the ratio of wire period to cross-section circumference $a/2\pi a_{\mathrm{sphere}}$ is larger for the smaller sphere. As a result, the small sphere has a relatively rougher surface than the larger sphere, resulting in something of a "stair casing" effect.

V. Effect of Wire Period: Breakdown of Homogenization

The derivation of the equivalent diffusion parameter and conductivity of the ICWM in [15] is based on the ICWM permittivity [1]. This is derived assuming that $ka \ll \pi$ where a is the wire lattice period and k is the wave number. The Bragg condition $ka \ll \pi$ leads to $a \ll c/2f$, which leads to the Bragg frequency $f_B = c/2a$. We expect the homogenized model to break down as the wire period increases enough to violate this Bragg condition. Furthermore, it is discussed in [15] that (10) looses accuracy above the effective plasma frequency (13) [although a more complicated nonlocal permittivity can be used instead of (10), restoring accuracy above the plasma frequency [1], here we simply use (10)]. In the following, different wire periods are considered and measurement results demonstrate that the homogenization approximation indeed starts to breakdown with increasing period, as expected.

To consider the breakdown of the homogenized isotropic permittivity, Fig. 15 shows measurement results for the D50a8d2, D50a12d2, and D50a12d2C spheres for the incident wave angle $\theta = \varphi = 45^\circ$ (wires are parallel to x, y, and z axes). Although not previously discussed, for the smaller period ($a = 4$ mm) spheres considered above the angle of the incident wave with respect to the wire orientation did not affect the measurement results, verifying that the material acts like an isotropic wire medium as expected (this is discussed in further detail below). However, for larger periods this is not the case, and so here we specify the orientation angle with respect to the wire axes. Comparing with Fig. 13, it is evident from Fig. 15 that for larger wire periods the agreement between theory and measurement becomes poorer at a much lower frequency than for the $a = 4$ mm wire sphere, due to the lower plasma and Bragg frequencies. For $a = 8$ mm and $d = 2$ mm these are $f_p = 16.56$ GHz and $f_B = 18.75$ GHz, and for $a = 12$ mm and $d = 2$ mm, $f_p = 9.13$ GHz and $f_B = 12.5$ GHz. For comparison, in Fig. 13 where the homogenization model is valid parameters are $a = 4$ mm, $d = 1$ mm, $f_p = 33.12$ GHz, and $f_B = 37.5$ GHz. Similarly, in Fig. 14, $a = 4$ mm, $d = 1$ mm, $f_p = 57.45$ GHz, and $f_B = 37.5$.

Finally, we consider the angle dependence of the wire medium spheres. Fig. 16 shows the measured extinction cross section for the D50a8d2, D50a12d2, and D50a12d2C spheres for different angles of the incident field with respect to the wire orientation. Two wire orientations are considered, $\theta = 0^\circ$ and $\theta = \varphi = 45^\circ$ (wires are aligned along the x, y, and $z$axes). Clearly, for the larger period spheres there is considerable angle dependence, whereas for the $a = 4$ mm period sphere there is

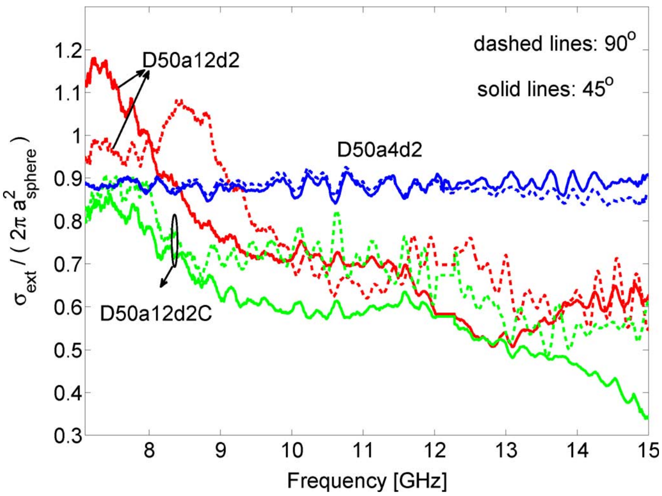

Fig. 16. Normalized measured extinction cross section of the D50a4d2, D50a8d2, D50a12d2, and D50a12d2C spheres showing the angle dependence for the spheres having larger periods.

no angle dependence except at the highest measurement frequencies. Furthermore the D50a12d2, and D50a12d2C spheres, which have the same wire period and diameter but differ in their wire placement, show different responses. Again, this is indicative of a breakdown of homogenization theory when frequencies approach the plasma and Bragg frequencies.

VI. Conclusion

A new integro-differential equation was proposed for solving scattering problems involving wire media, allowing the first treatment of three-dimensional wire medium objects. The integro-differential equation was shown to be efficient and accurate via comparisons with other results for the 2-D case, and nonlocal Mie theory and measurements for the 3-D case. In the 1-D case the integro-differential equation led to an analytical solution. For 3-D spheres, the effect of wire period and diameter was investigated experimentally in a range of parameters that demonstrated the expected breakdown of homogenization for large wire period.

Appendix

A. Proof of (24)

Reducing (19)–(21) to one dimension,

$$J_{\mathrm{c}}(z) = \sigma[E^{sca}(z) + E^{i}(z)] + \frac{D}{j\omega}\frac{d^2}{dz^2}J_{\mathrm{c}}(z),$$
$$J_{\mathrm{p}}(z) = j\omega\varepsilon_0(\varepsilon_r - 1)[E^{sca}(z) + E^{i}(z)]. \tag{46}$$

Using (70) and (71) of [15], (21) simplifies to

$$E^{sca}(z) = -\frac{J_{\mathrm{c}}(z) + J_{\mathrm{p}}(z)}{j\omega\varepsilon_0} \tag{47}$$

and upon substituting (47) into (19) and (20) and simplifying,

$$\frac{d^2}{dz^2}J_{\mathrm{c}} - \frac{\sigma + j\omega\varepsilon_0\varepsilon_r}{\varepsilon_0\varepsilon_r D}J_{\mathrm{c}} + \frac{j\omega\sigma}{\varepsilon_r D}E^{\mathrm{inc}} = 0. \tag{48}$$

The solution of (48) subject to the boundary condition $J_{\mathrm{c}}(-L) = J_{\mathrm{c}}(L) = 0$ is (23), from which (24) is found by use of the continuity equation.

B. 2-D Coupled Polarization and Conduction Currents

For the case of a conduction and polarization response, the reduction of (19)–(21) to two-dimensions is

$$\begin{aligned}\frac{J_y^{eq}(z) - J_y^{c}(z)}{j\omega\epsilon_0(\varepsilon - \varepsilon_1)} &= E_y^{i}(z) + \frac{(k_1^2 - k_y^2)}{j\omega\epsilon_0\varepsilon_1}\int_0^L g(z,z')J_y^{eq}(z')\,dz' \\ &\quad + \frac{q_y}{\omega\epsilon_0\varepsilon_1}\frac{\partial}{\partial z}\int_0^L g(z,z')J_z^{eq}(z')\,dz' \end{aligned} \tag{49}$$

$$\begin{aligned}\frac{J_z^{eq}(z) - J_z^{c}(z)}{j\omega\epsilon_0(\varepsilon - \varepsilon_1)} &= E_z^{i}(z) + \frac{k_y}{\omega\epsilon_0\varepsilon_1}\frac{\partial}{\partial z}\int_0^L g(z,z')J_y^{eq}(z')\,dz' \\ &\quad + \frac{1}{j\omega\epsilon_0\varepsilon_1}\left(k_1^2 + \frac{\partial^2}{\partial z^2}\right)\int_0^L g(z,z')J_z^{eq}(z')\,dz' \end{aligned} \tag{50}$$

where $\mathbf{J}^{\mathrm{eq}} = \mathbf{J}^{\mathrm{c}} + \mathbf{J}^{\mathrm{p}}$. The basis functions used were

$$J_y^{c} = \sum_{n=-N}^{N} a_y e^{jn\frac{\pi}{L}\left(z-\frac{L}{2}\right)} \tag{51}$$

$$J_z^{con} = \sum_{n=-N}^{N} a_z e^{jn\frac{\pi}{L}\left(z-\frac{L}{2}\right)}. \tag{52}$$

C. Scalar Functions (38) and (39)

In [32] it is shown that if ψ_ρ, $\psi_{E,H}$ are eigenvectors of the scalar Helmholtz equation with eigenvalues of α and k_{tr}, respectively, then $\mathbf{M}$, $\mathbf{N}$, and $\mathbf{L}$ function as in (35)–(37) will form a complete set of functions in their respective space of functions satisfying the same boundary conditions (note that the pilot vector is set to be $\hat{\mathbf{r}}$). Also, [32]

$$\nabla\times\nabla\times\mathbf{F} - k_{\mathrm{tr}}^2\mathbf{F} = 0; \quad \mathbf{F} = \mathbf{M},\mathbf{N} \tag{53}$$
$$\mathbf{L} = \nabla\psi_\rho; \quad \nabla^2\psi_\rho - \alpha^2\psi_\rho = 0. \tag{54}$$

Therefore, we need to show

$$\alpha = -\frac{\sigma + j\omega\epsilon_0\varepsilon}{\epsilon_0\varepsilon D} \tag{55}$$

$$k_{\mathrm{tr}}^2 = \omega^2\mu\epsilon_0\left(\varepsilon - j\frac{\sigma}{\omega\epsilon_0}\right). \tag{56}$$

Starting from the drift diffusion equation (17) and using Maxwell's equations, it is straightforward to show

$$\nabla^2\rho + \frac{\sigma + j\omega\epsilon_0\varepsilon}{\epsilon_0\varepsilon D}\rho = 0 \tag{57}$$

$$\nabla\times\nabla\times\mathbf{H} - \omega^2\mu\epsilon_0\left(\varepsilon - j\frac{\sigma}{\omega\epsilon_0}\right)\mathbf{H} = 0 \tag{58}$$

$$\nabla\times\nabla\times\mathbf{E} - \omega^2\mu\epsilon_0\left(\varepsilon - j\frac{\sigma}{\omega\epsilon_0}\right)\mathbf{E} = j\omega\mu D\nabla\rho. \tag{59}$$

By comparing (58) with (53), it is evident that k_{tr} is (56) since $\mathbf{H}$ can be expanded in terms of $\mathbf{M}$ and $\mathbf{N}$ functions.

If we substitute $\mathbf{L}$ for $\mathbf{E}$ in (59) (we can do this since the $\mathbf{M}$ and $\mathbf{N}$ functions in the $\mathbf{E}$ expansion make the left hand side of (59) zero),

$$\mathbf{L} = \frac{D}{\sigma + j\varepsilon\omega}\nabla\rho \tag{60}$$

and using (54)

$$\nabla\psi_\rho = \frac{D}{\sigma + j\varepsilon\omega}\nabla\rho \tag{61}$$

so that

$$\psi_\rho \propto \rho. \tag{62}$$

Comparing (62), (57), and (54) results in (55).

D. Solution of (18)

Since the basis functions in (44) are obtained so that they satisfy the wave equation for nonlocal materials, we can solve (18) for one component (for example, the θ or φ component) to obtain the unknown coefficients in (44). Here we pick the θ directed component for two reasons:

1) none of the terms in (18) will be set to zero;
2) the depolarizing dyadic contribution vanishes (as shown below), simplifying the calculation.

The dyadic Green's function is

$$\begin{aligned}\underline{\mathbf{G}}_{\mathrm{ee}}(\mathbf{r},\mathbf{r}') &= \left\{(3\hat{\mathbf{R}}\hat{\mathbf{R}} - \underline{\mathbf{I}})\left(\frac{1}{k^2R^2} - \frac{1}{jkR}\right) - (\hat{\mathbf{R}}\hat{\mathbf{R}} - \underline{\mathbf{I}})\right\}\\ &\quad\times\frac{e^{-jkR}}{4\pi R} - \underline{\mathbf{L}}\frac{\delta(\mathbf{r}-\mathbf{r}')}{k^2}\end{aligned} \tag{63}$$

where $\mathbf{R} = \mathbf{r} - \mathbf{r}'$. In the volume integral in (18), if we find the principal value of the integral by excluding a disc with thickness 2δ around point the $\mathbf{r}$ inside the sphere of radius a_{sphere}, the integrals become $(\int_0^{r-\delta} + \int_{r+\delta}^{a_{\mathrm{sphere}}})\int_0^{\pi}\int_0^{2\pi}\ldots\,d\varphi\,d\theta\,dr$, and the depolarizing dyadic will be [33] $\underline{\mathbf{L}} = \hat{\mathbf{r}}\hat{\mathbf{r}}$, and therefore $\underline{\mathbf{L}}\cdot\mathbf{J}_{\mathrm{c}}^{\theta}(\mathbf{r}) = 0$.

Plugging (44) into (18) and simplifying, we have

$$\begin{aligned}\mathbf{J}_{\mathrm{c}}(\mathbf{r})\cdot\hat{\theta} &+ \sum_n\left(c_{3n}\frac{D\alpha^2}{j\omega}\mathbf{L}(\mathbf{r},n)\cdot\hat{\theta}\right)\\ &+ j\omega\mu\sigma\left(\int\hat{\theta}\cdot\underline{\mathbf{G}}_{\mathrm{ee}}(\mathbf{r},\mathbf{r}')\cdot\mathbf{J}_{\mathrm{c}}(\mathbf{r}')\,dV'\right)\\ &= \sigma E_i^{\theta}(r,\theta)\end{aligned} \tag{64}$$

in which

$$\begin{aligned}\mathbf{M}(\mathbf{r},n) &= \frac{\cos(\varphi)}{\sin(\theta)}P_n^1(\cos(\theta))j_n(\rho)\hat{\theta}\\ &\quad - \sin(\varphi)\frac{dP_n^1(\cos(\theta))}{d\theta}j_n(\rho)\hat{\varphi}\end{aligned} \tag{65}$$

$$\begin{aligned}\mathbf{N}(\mathbf{r},n) &= \frac{j_n(\rho)}{\rho}\cos(\varphi)n(n+1)P_n(\cos(\theta))\hat{r}\\ &\quad + \frac{\cos(\varphi)dP_n^1(\cos(\theta))}{\rho d\theta}\frac{d}{d\rho}[\rho j_n(\rho)]\hat{\theta}\\ &\quad - \frac{\sin(\varphi)P_n^1(\cos(\theta))}{\rho\sin(\theta)}\frac{d}{d\rho}[\rho j_n(\rho)]\hat{\varphi}\end{aligned} \tag{66}$$

$$\begin{aligned}\mathbf{L}(\mathbf{r},n) &= \frac{d}{d\rho_t}[j_n(\rho_t)]\cos(\varphi)P_n^1(\cos(\theta))\hat{r}\\ &\quad - \frac{j_n(\rho_t)\sin(\varphi)}{\rho_t\sin(\theta)}P_n^1(\cos(\theta))\hat{\varphi}\\ &\quad + \frac{1}{\rho_t}j_n(\rho_t)\cos(\varphi)\frac{dP_n^1(\cos(\theta))}{d\theta}\hat{\theta}\end{aligned} \tag{67}$$

$$\rho = k_{tr}r, \quad \rho_t = \alpha r. \tag{68}$$

E. Nonlocal Mie Coefficients

The nonlocal Mie coefficients from [26] are

$$\begin{aligned}a_n &= \frac{-j_n(\theta_h)\theta_{\mathrm{tr}}j_n'(\theta_{\mathrm{tr}}) + j_n(\theta_{\mathrm{tr}})\theta_h j_n'(\theta_h)}{h_n^{(+)}(\theta_h)\theta_{\mathrm{tr}}j_n'(\theta_{\mathrm{tr}}) - j_n(\theta_{\mathrm{tr}})\theta_h\left[h_n^{(+)}(\theta_h)\right]'}\\ b_n &= \frac{-\varepsilon_h j_n(\theta_h)\left([\theta_{\mathrm{tr}}j_n(\theta_{\mathrm{tr}})]' + g_n\right) + \varepsilon_{tr}j_n(\theta_{\mathrm{tr}})[\theta_h j_n(\theta_h)]'}{h_n^{(+)}(\theta_h)\varepsilon_h\left([\theta_{\mathrm{tr}}j_n(\theta_{\mathrm{tr}})]' + g_n\right) - j_n(\theta_{\mathrm{tr}})\varepsilon_{\mathrm{tr}}\left[\theta_h h_n^{(+)}(\theta_h)\right]'}\end{aligned} \tag{69}$$

in which

$$g_n = \frac{n(n+1)j_n(\theta_{\mathrm{tr}})j_n(q_0a_{\mathrm{sphere}})}{q_0 a j_n'(q_0a_{\mathrm{sphere}})}\left(\frac{\varepsilon_{tr}}{\varepsilon_b} - 1\right) \tag{70}$$

$$q_0 = \sqrt{\frac{\sigma + j\omega\epsilon_0\varepsilon_b}{-D\epsilon_0\varepsilon_b}}; \quad \varepsilon_{\mathrm{tr}} = \varepsilon_b - j\frac{\sigma}{\omega\varepsilon_0} \tag{71}$$

where $\theta_{\mathrm{tr}} = k_0A\sqrt{\varepsilon_{\mathrm{tr}}}$, $\theta_h = k_0A\sqrt{\varepsilon_h}$, and a_{sphere} is the radius of the sphere, ε_b is the relative permittivity of the dielectric host environment of the wires, ε_h is the relative permittivity of the medium surrounding the sphere, j_n is the spherical Bessel function, and $h_n^{(+)}$ is the spherical Hankel function of the second kind. The usual local Mie theory is obtained by setting $g_n = 0$.

ACKNOWLEDGMENT

The authors would like to thank Mário Silveirinha from Pólo II da Universidade de Coimbra for his valuable comments and correspondence and Thomas Albert Beller from The University of Wisconsin-Milwaukee for his help in fabrication of the wire medium spheres.

REFERENCES

[1] M. G. Silveirinha, "Artificial plasma formed by connected metallic wires at infrared frequencies," *Phys. Rev. B*, vol. 79, pp. 035118(1)–0351181(15), 2009.

[2] W. Rotman, "Plasma simulation by artificial dielectrics and parallel-plate media," *IRE Trans. Antennas Propag.*, vol. AP-10, no. 1, pp. 82–95, Jan. , 1962.

[3] J. Brown, "Artificial dielectrics," in *Progress in Dielectrics*, J. B. Birks, Ed. New York, NY, USA: Wiley, 1960, pp. 193–225.
[4] J. M. Pitarke, F. J. Garcia-Vidal, and J. B. Pendry, "Effective medium response of a system of metallic cylinders," *Phys. Rev. B*, vol. 57, pp. 15261–15288, 1998.
[5] P. A. Belov, R. Marqués, S. I. Maslovski, I. S. Nefedov, M. Silveirinha, C. R. Simovski, and S. A. Tretyakov, "Strong spatial dispersion in wire media in the very large wavelength limit," *Phys. Rev. B*, vol. 67, pp. 113103-(1)–113103-(4), 2003.
[6] T. A. N. Morgado, "Tailoring the near- and far- fields with wire Media" Ph.D. dissertation, Univ, of Combria, Combria, Portugal, 2011 [Online]. Available: http://hdl.handle.net/10316/20348
[7] W. T. Lu and S. Sridhar, "Superlens imaging theory for anisotropic nanostructured metamaterials with broadband all-angle negative refraction," *Phys. Rev. B*, vol. 77, pp. 233101-(1)–233101-(4), 2008.
[8] P. Belov and M. G. Silveirinha, "Resolution of subwavelength transmission devices formed by a wire medium," *Phys. Rev. E*, vol. 73, pp. 056607-(1)–056607-(9), 2006.
[9] M. G. Silveirinha, P. Belov, and C. R. Simovski, "Subwavelength imaging at infrared frequencies using an array of metallic nanorods," *Phys. Rev. B*, vol. 75, pp. 035108-(1)–035108-(12), 2007.
[10] C. S. R. Kaipa, A. B. Yakovlev, S. I. Maslovski, and M. G. Silveirinha, "Near-field imaging with a loaded wire medium," *Phys. Rev. B*, vol. 86, pp. 155103-(1)–155103-(10), 2012.
[11] I. S. Nefedov, D. Chicherin, and A. J. Viitanen, "Infrared cloaking based on wire media," in *Proc. SPIE*, 2008, vol. 6987, p. 698728.
[12] G. Lovat, P. Burghignoli, and S. Celozzi, "Shielding properties of a wire-medium screen," *IEEE Trans. Electromagn. Compat.*, vol. 50, no. 1, pp. 80–88, Feb. 2008.
[13] S. Hrabar, "Application of wire media in antenna technology," in *Metamaterials and Plasmonics: Fundamentals, Modeling, Applications, NATO Science for Peace and Security Series B: Physics and Biophysics*. New York, NY, USA: Springer, 2009, pp. 139–151.
[14] P. Burghignoli, G. Lovat, F. Capolino, D. R. Jackson, and D. R. Wilton, "Directive leaky-wave radiation from a dipole source in a wire-medium slab," *IEEE Trans. Antennas Propag.*, vol. 56, no. 5, pp. 1329–1338, May 2008.
[15] G. W. Hanson, E. Forati, and M. G. Silveirinha, "Modeling of spatially-dispersive wire media: Transport representation, comparison with natural materials, and additional boundary conditions," *IEEE Trans. Antennas Propag.*, vol. 60, no. 9, pp. 4219–4239, Sep. 2012.
[16] G. W. Hanson, "Drift-diffusion: A model for teaching spatial dispersion concepts and the importance of screening in nanoscale structures," *IEEE Antennas Propag. Mag.*, vol. 52, no. 5, pp. 198–207, Oct. 2010.
[17] S. I. Maslovski and M. G. Silveirinha, "Nonlocal permittivity from a quasistatic model for a class of wire media," *Phys. Rev. B*, vol. 80, pp. 245101-(1)–245101-(10), 2000.
[18] G. W. Hanson, "Modeling of nonlinear, spatially-dispersive plasmas and semiconductors under harmonic excitation," *IEEE Trans. Antennas Propag.*, vol. 61, no. 2, pp. 779–787, Feb. 2013, "," Jan. 2012.
[19] G.W. Hanson, M.G. Silveirinha, P. Burghignoli, and A.B. Yakovlev, "Nonlocal susceptibility of the wire medium in the spatial domain considering material boundaries," *New J. Phys.*, 2013, submitted for publication.
[20] W. C. Chew, *Waves and Fields in Inhomogeneous Media*. Piscataway, NJ, USA: IEEE Press, 1995.
[21] A. Sihvola, *Electromagnetic Mixing Formulae and Applications*, ser. IEE Electromagnetic Wave series. London, U.K.: , 1999.
[22] M. G. Silveirinha and C. A. Fernandes, "Homogenization of 3-D-connected and nonconnected wire metamaterials," *IEEE Trans. Microw. Theory Tech.*, vol. 53, no. 4, pp. 1418–1430, Apr. 2005.
[23] J. L. Volakis and K. Sertel, *Integral Equation Methods for Electromagnetics*. Raleigh, NC: Scitech, 2012.
[24] M. G. Silveirinha, "Additional boundary condition for the wire medium," *IEEE Trans. Antennas Propag.*, vol. 54, no. 6, pp. 1766–1780, Jun. 2006.
[25] T. Shen and T. Wong, "Response of elementary semiconducting structures to a terahertz electric field," in *Proc. IEEE APS-URSI*, Chicago, IL, USA, Jul. 2011, pp. 1613–1616.
[26] C. David and F. J. García de Abajo, "Spatial nonlocality in the optical response of metal nanoparticles," *Phys. Chem. C*, pp. 19470–19475, May 2011.
[27] C. F. Bohren and D. R. Huffman, *Absorption and Scattering of Light by Small Particles*. New York, NY, USA: Wiley, 1983.
[28] R. G. Newton, "Optical theorem and beyond," *Amer. J. Phys.*, vol. 44, pp. 639–642, Jul. 1976.
[29] QWED Inc.. Warsaw, Poland, [Online]. Available: www.qwed.com.pl
[30] Structure Probe Inc., SPI Flash-Dry Silver Paint.
[31] Lumerical Solutions Inc., FDTD Solutions.
[32] W. C. Chew, *Waves and Fields in Inhomogeneous Media*. Piscataway, NJ, USA: IEEE Press, 1999.
[33] A. D. Yaghjian, "Electric dyadic Green's functions in the source region," *Proc. IEEE*, vol. 68, no. 2, pp. 248–263, Feb. 1980.

Ebrahim Forati (S'09) was born in Iran in 1983. He received the B.Sc. and M.Sc. degrees from Iran University of Science and Technology (IUST), Tehran, Iran, in 2006 and 2009, respectively. He is currently working towards the Ph.D. degree at the University of Wisconsin Milwaukee (UWM), Milwaukee, WI, USA.

He was a Research Assistant in the Electromagnetic Engineering Research Laboratory (EERL) at IUST and now is a Teaching Assistant at UWM. His current areas of research interests include electromagnetics and metamaterials.

George W. Hanson (S'85–M'91–SM'98–F'09) was born in Glen Ridge, NJ, USA, in 1963. He received the B.S.E.E. degree from Lehigh University, Bethlehem, PA, USA, in 1986, the M.S.E.E. degree from Southern Methodist University, Dallas, TX, USA, in 1988, and the Ph.D. degree from Michigan State University, East Lansing, MI, USA, in 1991.

From 1986 to 1988, he was a Development Engineer with General Dynamics in Fort Worth, TX, USA, where he worked on radar simulators. From 1988 to 1991, he was a Research and Teaching Assistant in the Department of Electrical Engineering at Michigan State University. He is currently Professor of Electrical Engineering and Computer Science at the University of Wisconsin Milwaukee (UWM), Milwaukee, WI, USA. His research interests include nanoelectromagnetics, mathematical methods in electromagnetics, electromagnetic wave phenomena in layered media, integrated transmission lines, waveguides, and antennas, and leaky wave phenomena. He is coauthor of the book *Operator Theory for Electromagnetics: An Introduction* (Springer, 2002) and author of *Fundamentals of Nanoelectronics*(Prentice-Hall, 2007).

Dr. Hanson is a member of URSI Commission B, Sigma Xi, and Eta Kappa Nu, and was an Associate Editor for the IEEE TRANSACTIONS ON ANTENNAS AND PROPAGATION from 2002 to 2007. In 2006 he received the S.A. Schelkunoff Best Paper Award from the IEEE Antennas and Propagation Society.